MASSACHUSETTS INSTITUTE OF TECHNOLOGY
Gravitation and Cosmology Research Group
Cambridge, Massachusetts 02139

MIT GRAVITY GRP. FAX #617-253-7014
CONFIRMATION # 617-253-4824

Facsimile Cover Sheet

DATE: 9.11.95 TIME: 2:00 pm (E.T.)

TO: Linda Turner FAX#: 818-304-9834

LIGO Project ADDRESS: Caltech

NUMBER OF PAGES (including this cover sheet): 30

FROM: Will Plummer OFFICE #: (617)253-4894

Massachusetts Institute of Technology
Room 20B-145
Cambridge, Massachusetts 02139

NOTES: Linda: If there are any problems please be in touch

Will

LASER INTERFEROMETER GRAVITATIONAL WAVE OBSERVATORY
- LIGO -

CALIFORNIA INSTITUTE OF TECHNOLOGY
MASSACHUSETTS INSTITUTE OF TECHNOLOGY

LIGO-T952009-00 -E 1 Jun95

Document Type *Doc Number* *Group-Id* *Date*

LIGO Optics specification: general concepts and constraints

Title

R. Weiss

Author(s)

DRAFT

This is an internal working note of the LIGO Project

Massachusetts Institute of Technology
LIGO Project - Rm 20B-145
Cambridge, MA 02139
Phone (617)253-4824
Fax (617)253-7014
E-mail: info@ligo.mit.edu
WWW: http://www.ligo.caltech.edu

DRAFT

March 3, 1994

BASIS OF THE OPTICAL WAVEFRONT SPECIFICATIONS

INTRODUCTION AND OVERVIEW

This document is intended to accompany *Surface Specifications for the LIGO Arm Cavity Mirrors* November 1, 1993.

Basic Assumptions: The large aperture optics (the recycling mirror, beam splitter and arm cavity mirrors) constitute the major untested extrapolation we are making from the laboratory scale interferometers to the LIGO. These optics will not be integrated into a gravitational wave interferometer until the initial LIGO interferometer is assembled in the LIGO facilities. The strategy we have adopted to minimize the risk of failure is to couple metrology of the optics to physical optical models of the interferometer and stray light models of the LIGO beam tubes. A variety of analytic and computer models of the interferometer have been developed for this purpose as well as analytic and computational stray light propagation models of the LIGO beam tubes.

Although it may be uncomfortable to rely so on models, no compelling arguments have been presented for intermediate length tests of the full scale optics in either the current prototypes or in ancillary intermediate baseline facilities such as the X-ray collimation tube at NASA, Huntsville, Alabama. The metrology is expected to be good enough to predict the optical performance on the spatial and angular scales relevant to the LIGO.

Basis of the specifications: The specifications for the large aperture optics of the initial LIGO interferometer are based on a combination of technical and scientific criteria strongly weighted by our expectations of the near term capabilities of the optics industry.

The goal for the initial interferometer is to achieve an rms strain sensitivity of 10^{-21} in a band of a few hundred Hz near a hundred Hz. We have chosen to use existing ion lasers with single mode output power of a few watts. Having set this goal and made the choice of the laser source, the interferometer must be a recycled system and the mirror properties become derived requirements.

The interferometer phase sensitivity is determined by the interferometer transfer function relating optical phase, $\phi(f)$, at the antisymmetric port to the gravitational wave strain, $h(f)$, incident on the interferometer.

$$\frac{\phi(f)}{h(f)} = \frac{4\pi\tau_{st}}{\tau_{opt}\sqrt{(1+(4\pi\tau_{st}f)^2)}}$$

$$\tau_{st} = \frac{2L}{c\,(T_{arminput} + L_{singlepass})}$$

The optical loss in an arm cavity is

$$L_{arm} = \frac{4\,L_{singlepass}}{T_{arminput}}$$

The phase noise due to quantum fluctuations in the light and photodetection with power recycling is given approximately by (a more complete expression including the RF modulation is given in *Analysis of an Externally Modulated Recycled Interferometer* D. Shoemaker and R. Weiss):

$$\phi_n^2(f) \approx \frac{h\nu L_{\rm total}}{C\eta P_{\rm input}(1-L_{\rm arm})} \qquad L_{\rm total} = L_{\rm arm} + L_{\rm rcyl} + (1-C)$$

where C is the fringe contrast at the antisymmetric port.

The equivalent gravitational wave strain noise becomes

$$h_n(f) = \frac{h(f)}{\phi(f)}\,\phi_n(f)$$

Sample Parameters

$T_{\rm arminput}$	3×10^{-2}
$\tau_{\rm st}$	9×10^{-4} sec
$\tau_{\rm opt} = \lambda/c$	1.7×10^{-15} sec
$L_{\rm arm}$	$< 3\times10^{-2}$
$L_{\rm singlepass}$	$< 2.1\times10^{-4}$
$L_{\rm total} = T_{\rm rcyl}$	$< 4\times10^{-2}$
$1-C$	$< 3\times10^{-3}$
$\eta P_{\rm input}$	2 watts
$\phi_n(f)$	9×10^{-11} radians/$\sqrt{\rm Hz}$
$h(100{\rm Hz})$	$2\times10^{-23}1/\sqrt{\rm Hz}$

The arm cavity geometric parameters are set by the cavity g factors which determine the Guoy phase and with the wavelength determine the Gaussian spot radii.

$$g = 1 - \frac{L}{R}$$

where L is the cavity length and R is the radius of curvature of the curved mirror.

The Gaussian beam size on the flat mirror of the flat/spherical cavity is given by

$$w_0 = \sqrt{\frac{L\lambda}{\pi}}\left(\frac{g}{(1-g)}\right)^{1/4}$$

and on the curved mirror by

$$w = \sqrt{\frac{L\lambda}{\pi}}\left(\frac{1}{g(1-g)}\right)^{1/4}$$

In the spherical/spherical cavity the spot size at either mirror is

$$w = \sqrt{\frac{L\lambda}{\pi}}\left(\frac{1}{(1-g^2)}\right)^{1/4}$$

The Gaussian spot radii for the LIGO cavities are shown in figure 1 as a function of the curved mirror g factor. The diffraction power loss of the lower order Laguerre-Gauss cavity modes as a function of the ratio of aperture radius, r, to Gaussian spot size, w, is shown in figure 2. The power excitation of higher order Laguerre-Gauss modes by the diffraction of a finite aperture illuminated by a $TE_{0,0}$ mode is shown in figure 3.

The Guoy phase for the $TE_{0,0}$ mode is

$$\psi_{0,0} = \cos^{-1}(\sqrt{g_1 g_2})$$

and the difference between the Guoy phase of any other Laguerre-Gauss mode with radial index p and angular index m and the $TE_{0,0}$ mode is

$$\Delta\psi_{pm} = (2p + m)\psi_{0,0}$$

The cavity g factors are chosen so that the Guoy phase difference of modes with low values of p and m, modes that have small diffraction loss in the cavities, will not be multiples of $n2\pi$ and therefore resonant in the cavity simultaneously with the $TE_{0,0}$ mode.

The requirement on the contrast defect is not only based on the shot noise estimate for the signal to noise which varies slowly with the contrast defect, as shown in figure 4 (the figure includes the optimization of the modulation index to maintain the shot noise minimum), but is also determined by the allowed power on the photo detector at the antisymmetric port assumed to be less than 300 milliwatts, a qualitative estimate for the effect on the wavefront alignment system and a hedge against extrinsic amplitude noise of the laser. The minimum coating diameter is chosen to maintain the allowed contrast defect and arm cavity loss.

The adopted cavity and interferometer parameters are summarized in Table 1 and Table 2.

The wavefront distortion specifications assume that the initial interferometer will not use an output mode filter and that the spatial mode degeneracy of the recyling cavity composed of the recycling and two front cavity mirrors does not make a serious contribution to the loss of the RF sidebands in the recycling cavity.

The use of an output mode filter is a backup in the event that we have difficulty in achieving the wavefront specifications. The deleterious effects of the recycling cavity degeneracy are currently under investigation. Should further optical modeling indicate that the wavefront distortion of the RF sidebands is significant and plays an important role in compromising the wavefront sensing alignment system, the preference is not to increase demands on the mirror specifications. Rather, to remove the degeneracy by figured optics in the recycling cavity or to abandon the asymmetric interferometer configuration.

The requirements for cavity loss, contrast defect and phase noise due to scattering, are in many regards satisfied by optics used in small space based low scatter optical telescopes and microelectronics optical masking machines. The primary differences arise from the need to control wavefront distortion on passing through thick substrates and from the transmission and reflection by large aperture multilayer dielectric coatings.

TABLE 1
OVERALL INITIAL OPTICAL PARAMETERS

Optical wavelength: $\lambda = 5.145 \times 10^{-5}$ cm

Cavity geometric parameters:

Arm cavity length: $L_{\rm arm} = 4 \times 10^5$ cm
Recycling cavity length: $L_{\rm recyl} = 1.2 \times 10^3$ cm
Radius of arm cavity front mirror: $R_{\rm front\ arm} = R_1 = \infty$ (flat)
Radius of arm cavity back mirror: $R_{\rm back\ arm} = R_2 = 6 \times 10^5$ cm
Arm cavity g factor 1: $g_1 = 1.0$
Arm Cavity g factor 2: $g_2 = 0.333$
Gaussian spot radius at front: $\omega_0 = \omega_1 = 2.15$ cm
Gaussian spot radius at back: $\omega_2 = 3.73$ cm
Gouy phase of $TE_{0,0}$ mode in arm cavity: $\psi_{0,0} = 9.56 \times 10^{-1}$ radians
Closest mode $p \leq 5$, $m \leq 5$; $\Delta\psi_{5,3} = -0.14$ radians
Rayleigh range: $z_r = 2.83 \times 10^5$ cm
Radius of recycling mirror: $R_{\rm rcycl} = 6.64 \times 10^7$ cm (flat)
Recycling cavity g factor: $g = 1 - 1.8 \times 10^{-5}$ (almost unstable cavity)

Optical properties (scattering and losses):

Scattering and absorption loss of surfaces: $A \leq 1.0 \times 10^{-4}$
BRDF of surfaces: $\frac{dP_{\rm scat}}{d\Omega * P_{\rm inc}} \leq \frac{1 \times 10^{-6}}{\theta^2}$ sr^{-1}, $\theta \leq 6 \times 10^{-3}$ radians
(Value used in tube scattering model)
Loss coefficient of bulk material: $\alpha \leq 5 \times 10^{-6}$ cm^{-1}
Approximate rms surface error : $\frac{\sigma_{\rm rms}}{\lambda} \leq \frac{1}{400}$

Optical Properties (reflectivity and transmission):

Reflectivity of recycling mirror: $R_{\rm recyl} = 0.96 - A$
Reflectivity of front arm cavity mirror: $R_{\rm front\ arm} = 0.97 - A$
Transmission of back arm cavity mirror: $T_{\rm back\ arm} = 1 \times 10^{-5}$
Reflectivity of back arm cavity mirror: $R_{\rm back\ arm} = 1.0 - A - T_{\rm back\ arm}$
Reflectivity of beam splitter: $R_{\rm beam\ split} = 0.5 - A/2$
Transmission of beam splitter: $T_{\rm beam\ split} = 0.5 - A/2$

Cavity and Interferometer Performance Parameters

Arm cavity loss: $L_{\rm arm} \leq 2.7 \times 10^{-2}$
Contrast defect at antisymmetric port: $1 - C \leq 3 \times 10^{-3}$
Recycling cavity loss ($A_{\rm recyl}$, AR coatings, bulk loss): $L_{\rm rec} \leq 2 \times 10^{-3}$
Recycling power gain $= (L_{\rm arm} + (1 - C) + L_{\rm rec})^{-1}$: ≥ 30
Power on antisymmetric port photodetector: $P_{\rm det} \leq 300$ mW

Optics dimensions:

Arm cavity mirror diameter: $D = 25$ cm

Arm cavity mirror thickness: $t = 10$ cm

Minimum coating diameter front cavity mirror: $D_{ct1} = 12$ cm

Minimum coating diameter rear cavity mirror: $D_{ct2} = 20$ cm

Minimum coating diameter sph/sph arm cavity: $D_{ct} = 14.5$ cm

TABLE 2

OPTICAL POWER AND INTENSITY AT VARIOUS COMPONENTS

component	ω (cm)	Power (W)	Intensity (W/cm^2)
ϕ modulator	7×10^{-2}	4	4×10^2
isolator	5×10^{-2}	4	8×10^2
mode filter (flat)	1×10^{-1}	4×10^3	2×10^5
mode filter (curved)	2×10^{-1}	4×10^3	6×10^4
telescope out. mir.	2.1	3	4×10^{-1}
recycling mir.	2.1	8×10^1	1×10^1
beam splitter	2.1	8×10^1	1×10^1
arm cavity input mir.	2.1	4.5×10^3	6.7×10^2
arm cavity far mir.	3.8	4.5×10^3	2×10^2
main frame laser	5×10^{-2}	1×10^2	3×10^4

Extension from experience in the prototypes: There are several critical areas in the specification of the large aperture optics for the initial LIGO interferometer which change priorities from the experience with the current prototypes. The initial LIGO interferometer cavities have much lower finesse than those now in the 40 meter system and the interferometer will be optically recombined. Even though we intend to power recycle the interferometer, the planned recycling power gain is modest. These factors taken together make optical loss from all sources of comparable importance to contrast defect at the antisymmetric port of the interferometer and the scattering by the mirror, which can contribute to phase noise from the tube walls. The other change is the increase in Gaussian spot radius from mm to cm scales. The new issue affecting the interferometer performance becomes the more difficult to control "figure errors" rather than the small scale roughness of the surfaces, substrates and coatings. The problem is compounded by the experience that the spatial power spectrum of optical wavefront phase distortions have a $\frac{1}{\nu^n}$ dependence with n varying between 1 to 3 depending on the spatial frequency ν and fabrication procedures.

Wavefront characterizations

Power spectrum: Figure 5 shows a composite hypothetical one dimensional power spectrum of surface perturbations for a high quality small telescope mirror based on data from Hughes Danbury at low spatial frequencies and typical surface roughness measurements in the literature at high spatial frequencies. The spectrum is given in units of waves^2 (5145A) of optical distortion per wavenumber (cm^{-1}) of spatial frequency. The integral of the power spectrum over spatial frequency gives the mean square fluctuations of the wavefront in units of optical waves when surface correlations become negligible: typically, above 3 cm^{-1}. The high frequency power spectrum shown represents a high quality but not superpolished surface: microroughness of several Angstroms rather than fractions of an Angstrom. The one dimensional power spectrum above about 0.3 cm^{-1} varies as $\frac{1}{\nu}$. The two dimensional power spectrum varies as $\frac{1}{\nu^2}$ so that the differential scattering (BRDF) would vary as $\frac{1}{\theta^2}$ where θ is the scattering angle from the mirror normal. The sample spectrum would give a mirror with 130 ppm loss due to irregularities with spatial frequency larger than 3 cm^{-1}. The low spatial frequency errors would produce an interferometer contrast defect of $\approx 10^{-4}$ (front mirror) and $\approx 10^{-3}$ (back mirror) and equivalent overall cavity loss when such a mirror is put into a LIGO arm cavity. Over the Gaussian spot diameter the sample mirror would have a small spatial frequency rms of $\approx \frac{\lambda}{500}$.

The role of the different spatial frequencies of the wavefront perturbations is broadly indicated in the figure. Power at all spatial frequencies contribute to optical loss. The power at spatial frequencies between 0.1 to 3 cm^{-1} is particularly important in establishing the interferometer contrast defect. While the power between 3 to 125 cm^{-1} incurs scattering into angles that encounter the LIGO beam tube and baffles producing phase noise due to scattered light. The power in spatial frequencies larger than 125 cm^{-1} is scattered into large angles which is strongly attenuated by the beamtubes and also has a small probability of recombination with the main beam. This is the domain of microroughness which has been a major concern in the prototypes but is less important in the initial LIGO interferometer.

Figure 5 also shows the spatial frequency band and typical sensitivities of the available metrological techniques.

Orthogonal cylindrical functions: The spatial power spectrum is a useful quantitative measure for the differential scattering and the integrated scattering loss when one can neglect the spatial coherence of the exciting light and the correlations on the mirror surface: in our application for spatial frequencies larger than about 3 cm^{-1}. At spatial frequencies below 3 cm^{-1}, to estimate the performance of the cavities and the interferometer, it is more useful to expand the wavefront perturbations in terms of orthogonal cylindrical functions. We have chosen to express the low spatial frequency part of the mirror specifications in terms of Zernike and Laguerre - Gauss functions.

Zernike functions: The Zernike functions have become a standard in the optical industry. The lower order radial and angular Zernike functions are directly related to specific aberrations in the wavefront and optical shops have developed intuition for reducing their amplitude by adjusting polishing techniques.

There are several difficulties with using the Zernike functions, however. The first, trivial but confusing, is that the normalization of the functions has not been standardized so that one has to be careful to know the definitions used in the software associated with the wavefront decompositions. More relevant is that they have a poor weighting for our application.

The scale parameter for the Zernike functions is the aperture radius. The critical part of the wavefront in our application lies within about 3 Gaussian spot radii. A full mirror aperture Zernike decomposition, therefore, places the important terms at high radial order. This can in part be alleviated by reducing the aperture radius. The cavity optical modeling has shown that even with subaperatures, the dynamic range in radial order required to properly characterize the interferometer contrast defect is still larger than that available in most commercial software packages. In addition, the radial functions themselves, especially the higher order functions, have large derivatives at the aperture edges so that with a finite number of pixels in the wavefront map, the orthogonality of the functions is not maintained in practice. This results in the large amplitude terms corrupting the estimates for the small amplitude ones. Standard computational techniques for orthogonalizing a subset of the functions evaluated on a given pixel grid have been developed but are also not part of most of the software packages used in optical shops.

Laguerre- Gauss Functions: The Laguerre - Gauss functions are the cylindrical form of the Cartesian Hermite - Gauss functions. Both are solutions of the paraxial ray equations associated with the cavity modes of the interferometer and are thereby a natural basis to transform the wavefronts in our application. The key parameter becomes the Gaussian beam spot size and the wavefront distortions of the mirrors, expressed in terms of these transforms, are optimally weighted. Furthermore, the interferometer performance can be easily related analytically to the transform amplitudes when projected onto the input TE_{00} mode. The trouble with these functions is that they are not standard in the optical industry.

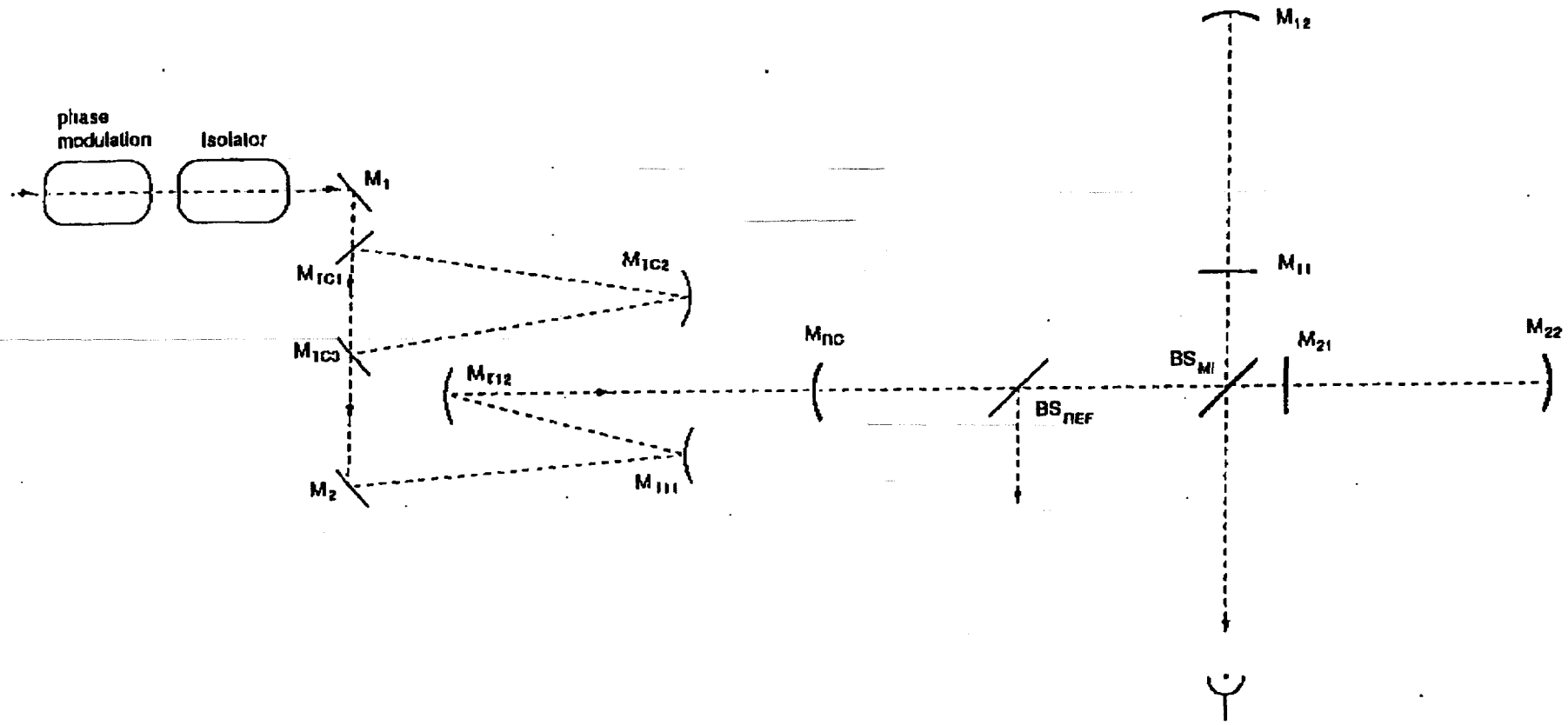

Initial interferometer optical schematic

FIG 6

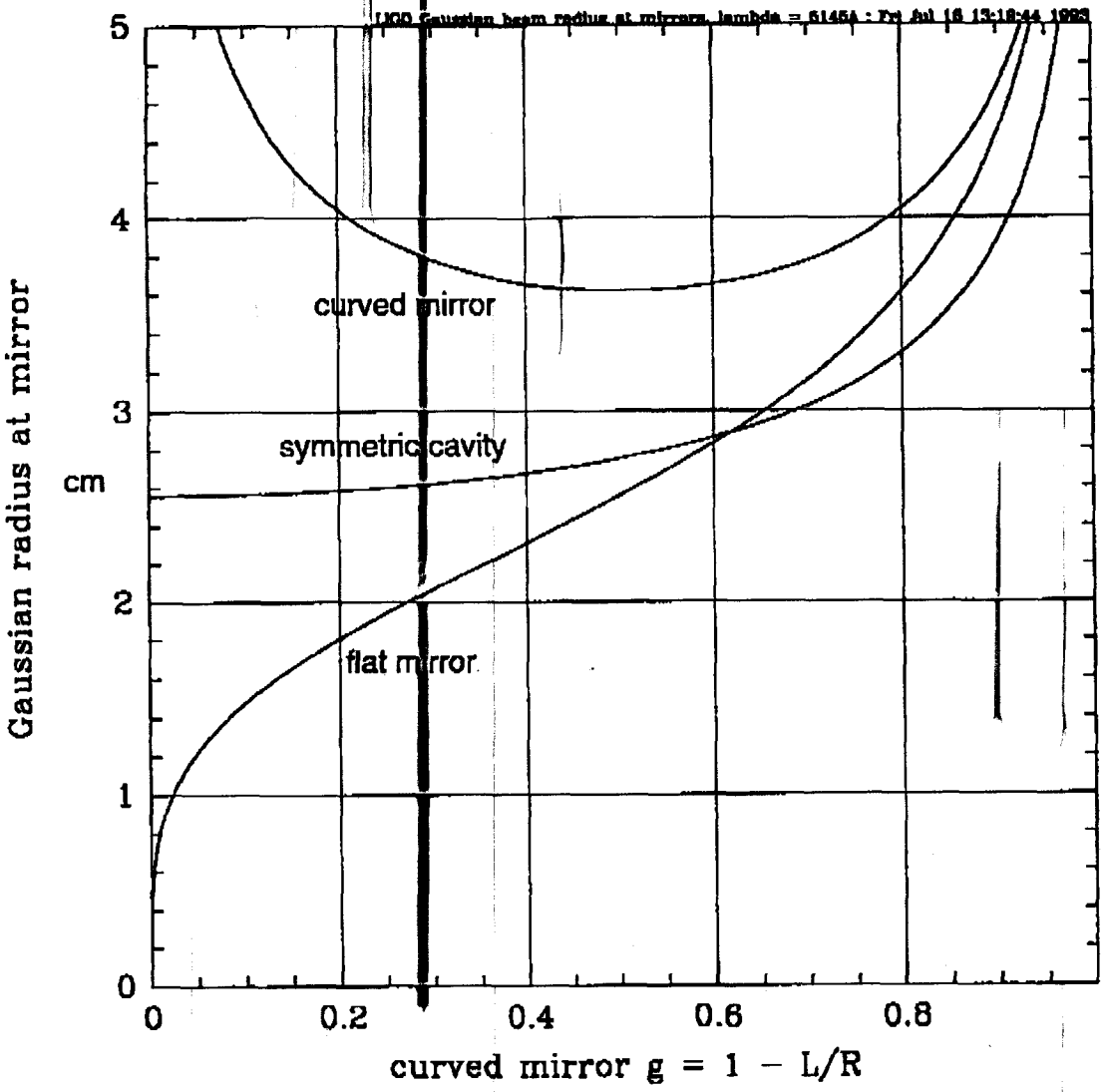
LIGO Gaussian beam radius at mirrors, lambda = 0.1454 : Fri Jul 28 15:18:44 1995
Gaussian radius at mirror
cm
5
4
3
2
1
0
curved mirror
symmetric cavity
flat mirror
0
0.2
0.4
0.6
0.8
curved mirror g = 1 − L/R

FIG 1

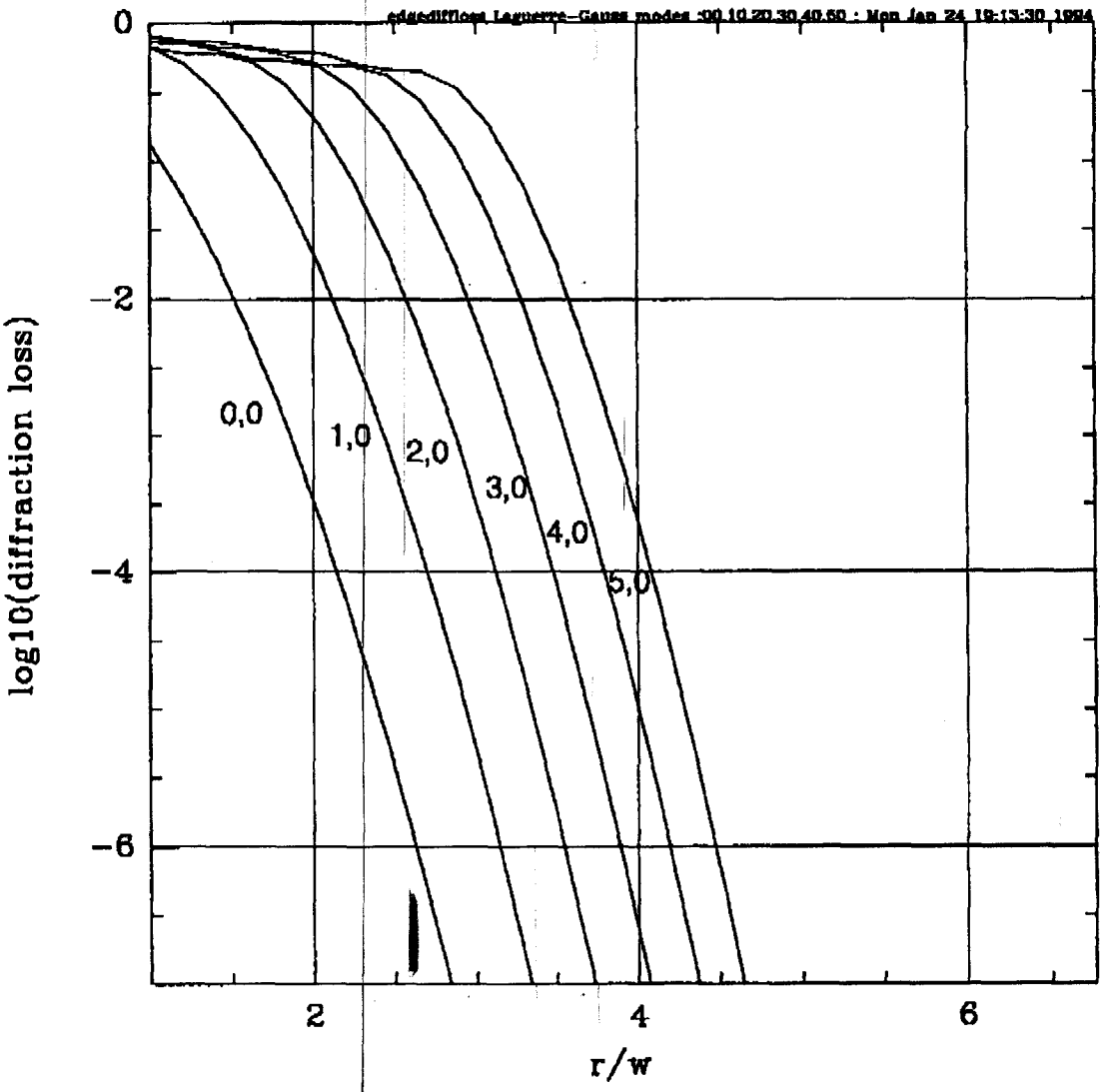
edgediffloss Laguerre-Gauss modes :00 10 20 30 40 60 : Mon Jan 24 19:13:30 1994
0
-2
-4
-6
log10(diffraction loss)
0,0
1,0
2,0
3,0
4,0
5,0
2
4
6
r/w

FIG 2

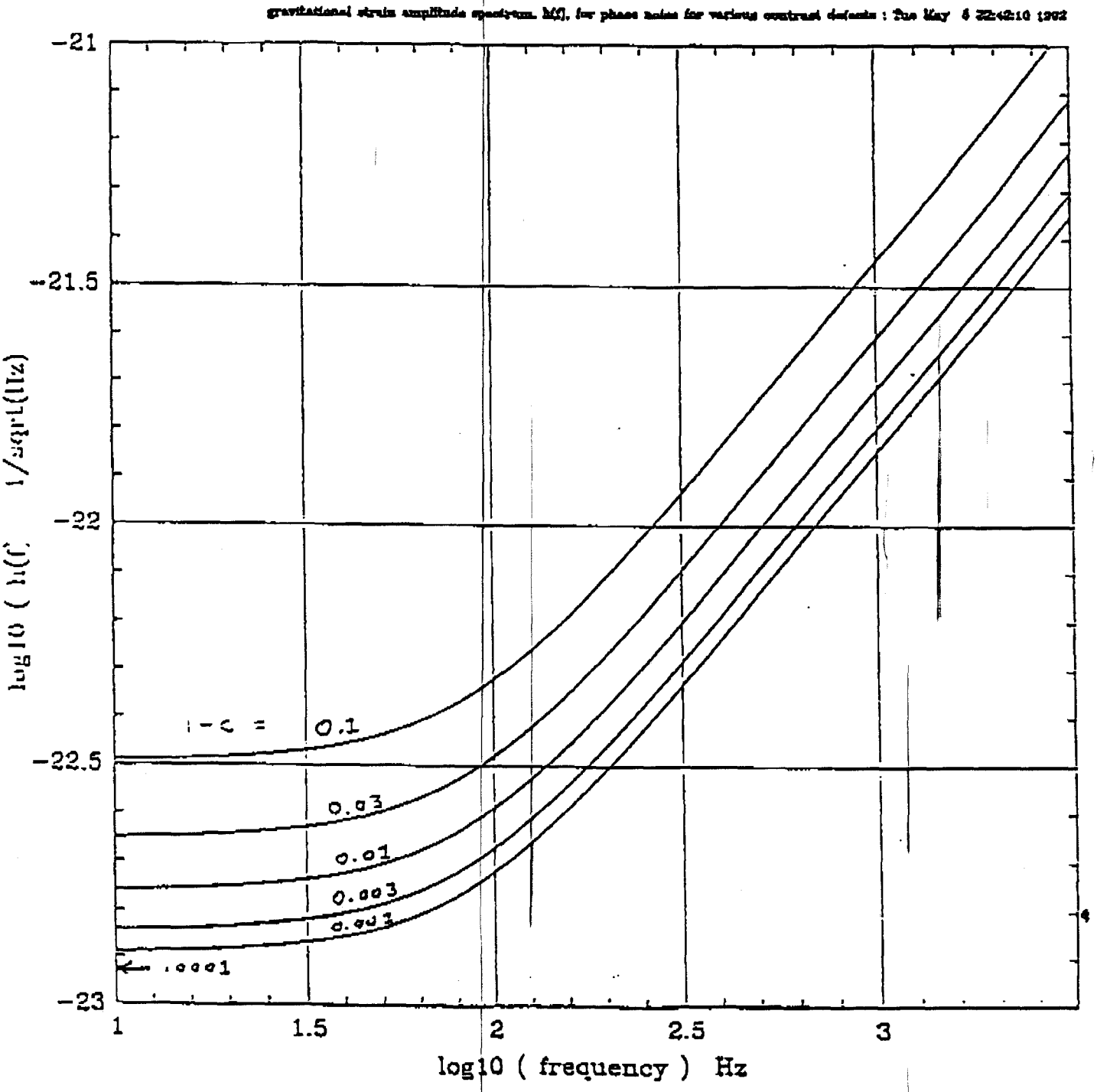
gravitational strain amplitude spectrum h(f), for phase noise for various contrast defects : Tue May 4 22:42:10 1982
-21
-21.5
-22
-22.5
-23
log10 (h(f) 1/sqrt(Hz)
1 - c = 0.1
0.03
0.01
0.003
0.001
.0001
1
1.5
2
2.5
3
log10 (frequency) Hz

FIG 4

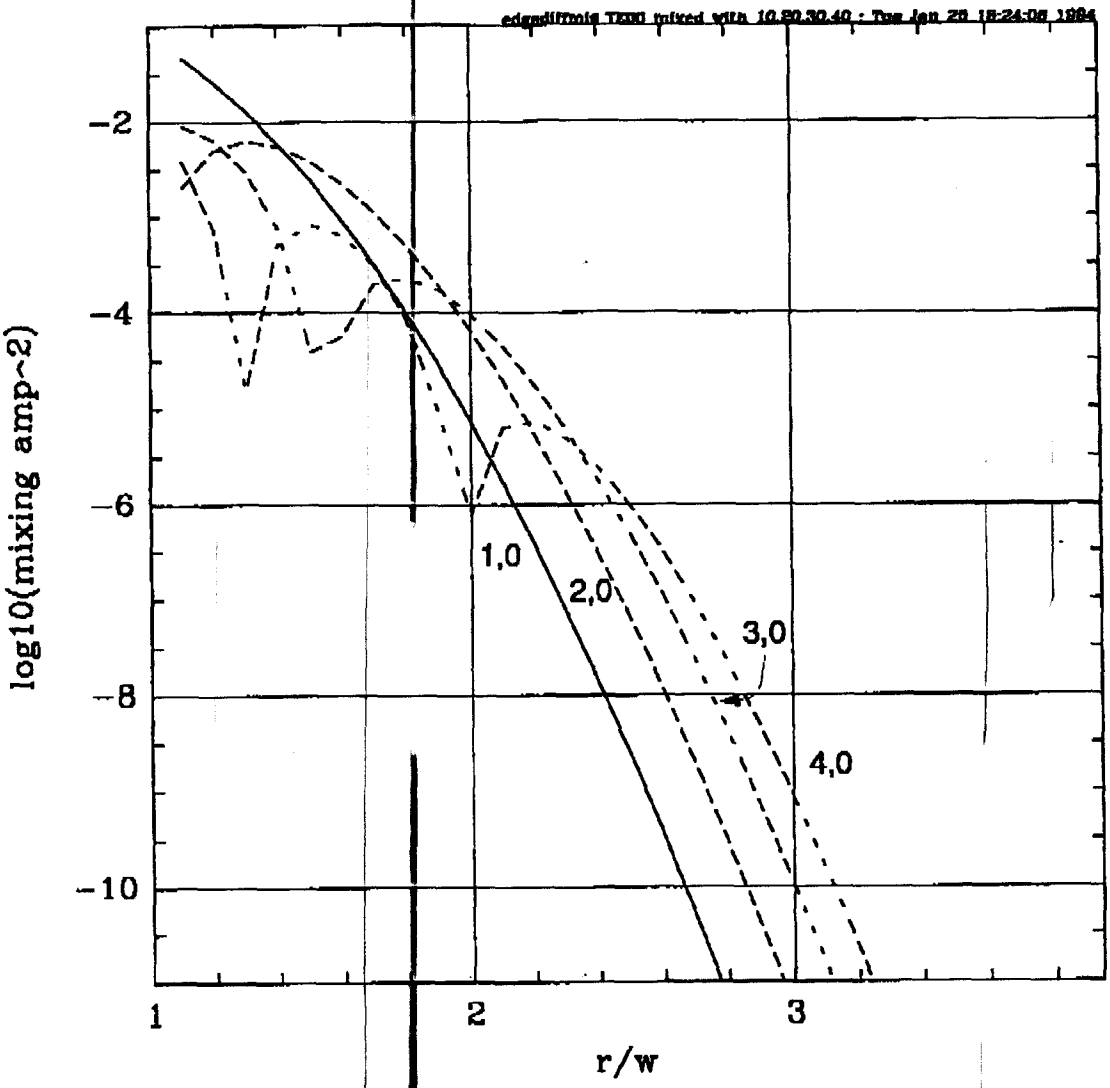
edgediffmois TEXT mixed with 10,20,30,40 : Tue Jan 28 18:24:06 1986
-2
-4
-6
-8
-10
log10(mixing amp^2)
1,0
2,0
3,0
4,0
1
2
3
r/w

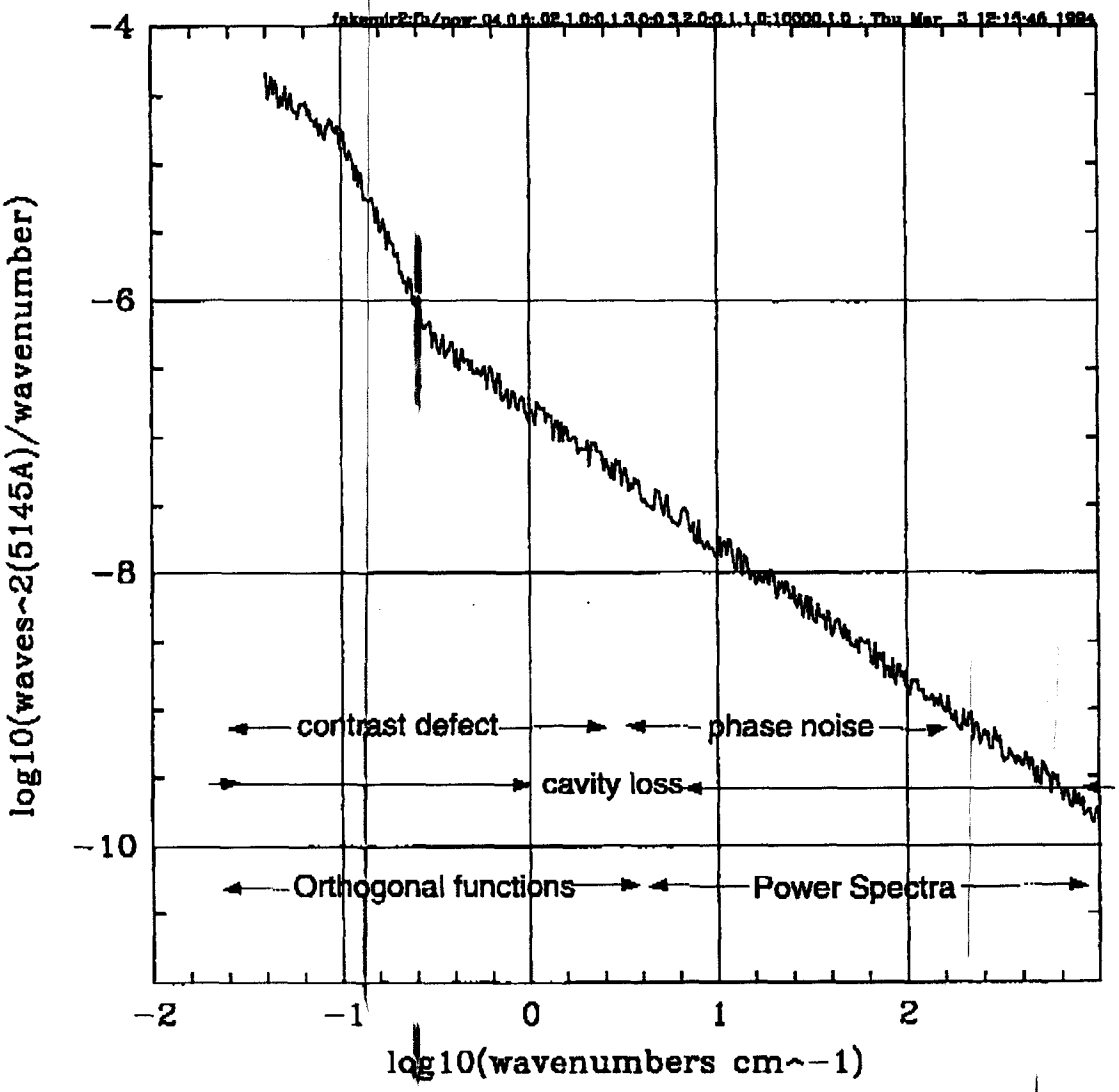
log10(waves~2(5145A)/wavenumber)
-4
-6
-8
-10
-2
-1
0
1
2
log10(wavenumbers cm~-1)
contrast defect
phase noise
cavity loss
Orthogonal functions
Power Spectra

FIG 5

TECHNIQUES TO MODEL THE CAVITIES AND THE INTERFEROMETER

Introduction: Two methods have been developed to calculate the cavity and interferometer performance from the measured wavefronts: the FFT paraxial ray propagation code and an approximate analytic technique that uses the orthogonal function transforms.

The FFT propagation code was developed by the VIRGO group and then improved by LIGO team members (P. Saha, Y. Hefetz and B. Bochner). The program calculates the complex optical field wavefronts directly by using the paraxial form of the Kirchoff diffraction integrals. The current pixel format is 128 by 128 so that the program is primarily useful for wavefront distortions at low spatial frequencies. Routines have been developed to converge on the field solutions in single cavities and a full recycled interferometer using guided iteration methods. The optical components are characterized by their phase maps in reflection (work is currently underway to include transmission phase maps). Once a field solution is determined by the main propagation program, auxiliary programs calculate the interferometer contrast and loss and modal decompositions of the fields, if these are desired.

The FFT propagation code is the best method we have for estimating the overall interferometer and cavity performance once the actual phase maps for the LIGO mirrors have been measured. The program will be the primary tool for making the final evaluation of the LIGO optics after metrology of the components.

The mirror specifications have been primarily determined by analytic perturbation techniques using single perturbed mirrors in modal expansions in a single cavity. The results were later spot checked for consistency with the FFT program. There are several reasons for this. The first is historical, the analytic techniques were developed before the FFT code became available. The second is that the computational efficiency of the analytic methods is much better than the FFT code, a typical Cray run with the FFT program takes about 15 minutes while an entire phase map can be analysed in a matter of seconds by the analytic methods. Finally, the analytic methods give some insight to the types of wavefront distortions significant in influencing the interferometer and cavity performance. The analytic methods,however, have not been developed to determine the performance of a full recycled interferometer.

One of the questions that was not addressed by the analytic methods was the overall contrast defect and loss with several perturbed mirrors in the interferometer. To establish the scaling relations for contrast defect and loss, the FFT program was used with perturbed but statistically similar mirrors at all locations in the interferometer. The results of these runs are that the contrast defect and loss grow linearly with the number of perturbed mirrors in the interferometer. The relation is only approximately true for the flat/spherical cavities where the beam size on the spherical mirror is larger than on the flat. In these cavities the spherical mirror is more critical than the flat to establish the overall cavity loss since the beam samples lower spatial frequencies on the mirror. For the contrast defect estimates this is partially offset by the spatial filtering of the cavity and the perturbation of the wavefront from the unfiltered reflection at the front flat mirror.

The analytic method and the mirror specification: The basis of the analytic method is to illuminate an imperfect optical component by a $TE_{0,0}$ mode field and to decompose the perturbed transmitted or reflected wave into a sum of Laguerre-Gauss mode fields. The modal fields are then propagated through the optical train to calculate the modal optical transfer function of the system. The calculation is carried out in first order: the modal fields are not decomposed iteratively after each encounter with a new perturbing component. In a cavity, for example, the perturbations due to the back mirror are calculated once as a source of the modal fields and then these fields are propagated in the cavity as though the optics were perfect. The cavity diffraction loss and Guoy phase for the modal field is included in the cavity transfer function for the mode. The method applies only for small wavefront perturbations. The loss of the cavity is estimated by calculating the ratio of the sum of the cavity intensities in the higher order modes to that of the cavity intensity in the exciting $TE_{0,0}$ mode. The contrast defect is determined by the ratio of twice the sum of the intensities in the higher modes to the intensity of the exciting $TE_{0,0}$ light in reflection.

The real Laguerre - Gauss functions are

$$LG_{p,m,+}(r,\theta) = \frac{M_{p,m}}{w_0}(\frac{\sqrt{2}r}{w_0})^m L_p^m(\frac{2r^2}{w_0^2})e^{-r^2/w_0^2}\cos(m\theta)$$

$$LG_{p,m,-}(r,\theta) = \frac{M_{p,m}}{w_0}(\frac{\sqrt{2}r}{w_0})^m L_p^m(\frac{2r^2}{w_0^2})e^{-r^2/w_0^2}\sin(m\theta)$$

where w_0 is the Gaussian waist radius and $L_p^m(\frac{2r^2}{w_0})$ are the Laguerre polynomials. The Laguerre-Gauss functions are ortho-normal

$$\int_0^\infty \int_0^{2\pi} LG_{p,m,\pm}(r,\theta)\, LG_{j,q,\pm}(r,\theta)\, r dr d\theta = \delta_{p,j}\delta_{m,q}$$

when the normalization constant is chosen as

$$M_{p,0} = (\frac{2p!}{\pi((m+p)!)^3})^{1/2}$$

$$M_{p,m} = (\frac{4p!}{\pi((m+p)!)^3})^{1/2}$$

The optical phase shift (without the 2π) of a perturbed reflecting surface or transmitting component is characterized by the height distribution in waves

$$\frac{z(r,\theta)}{\lambda}$$

derived from interferometric phase maps of the component. A spatial variation in the reflection or transmission amplitude is determined from intensity maps

$$r(r,\theta) = \sqrt{R(r,\theta)} \qquad t(r,\theta) = \sqrt{T(r,\theta)}$$

The Gaussian weighted decomposition components of the phase map are then defined as

$$b_{p,m,0,0,\pm} = \int_0^{\infty}\int_0^{2\pi} LG_{p,m,\pm}(r,\theta)\frac{z(r,\theta)}{\lambda}LG_{0,0}(r,\theta)r\,dr\,d\theta$$

with corresponding decompositions for the reflection and transmission amplitudes.

The interpretation of $b_{p,m,0,0,\pm}$ requires some care since even a perfect surface of finite radius will give non vanishing values due to the diffraction loss by the finite aperture. With the parameters of the LIGO cavities and mirror diameters, values of $b^2_{p,m,0,0,\pm} \leq 1\times10^{-7}$ on the spherical mirror and $b^2_{p,m,0,0,\pm} \leq 2\times10^{-15}$ on the flat mirror for $p \leq 20$ are limits due to the finite mirror size.

When the phase, transmission or reflection maps are expressed as Zernike functions over the measurement aperture, the procedure includes the added step of converting the Zernike transforms into the Gaussian Weighted Laguerre- Gauss decompositions.

The Zernike functions are area normalized and real - use sin and cos as the angular functions.

$$Z_{n,l,+}(r,\theta) = N_{n,l}\,R_{n,l}(r)\,\cos(l\theta)$$

$$Z_{n,l,-}(r,\theta) = N_{n,l}\,R_{n,l}(r)\,\sin(l\theta)$$

The $R_{n,l}$ are the radial Zernike functions.

The Zernike functions are ortho-normal

$$\int_0^{R}\int_0^{2\pi} Z_{n,l,\pm}(r,\theta)\,Z_{j,q,\pm}(r,\theta)\,r\,dr\,d\theta = \delta_{n,j}\delta_{l,q}$$

where R is the aperture radius. The normalization constant is chosen as

$$N_{n,0} = \sqrt{\frac{n+1}{\pi}}$$

$$N_{n,l} = \sqrt{\frac{2(n+1)}{\pi}}$$

The phase surface, $z(r,\theta)$, is decomposed

$$\frac{z(r,\theta)}{\lambda} = \sum_{0,0}^{n,l,\pm} a_{n,l,\pm}\,Z_{n,l,\pm}(r,\theta)$$

where the amplitude coefficients are defined as

$$a_{n,l,\pm} = \int_0^{R}\int_0^{2\pi} \frac{z(r,\theta)}{\lambda}Z_{n,l,\pm}(r,\theta)r\,dr\,d\theta$$

NOTE: The Zernike functions used in ZYGO interferometer software are not normalized. The functions all have $N_{n,l} = 1$ and are given by a numbering scheme from 1 to 36 that includes the real functions from $n = 0$, $l = 0$ to $n = 7$, $l = 7$.

The Gaussian weighted Zernike decomposition components become

$$b_{p,m,n,l,0,0,\pm} = \int_0^\infty \int_0^{2\pi} LG_{p,m,\pm}(r,\theta) a_{n,l,\pm} Z_{n,l,\pm}(r,\theta) LG_{0,0}(r,\theta) r\,dr\,d\theta$$

FORTRAN Programs Used in Determining the Specification

OPTICS:

cavmodes.f

Cavity mode maps

contloss.f

Cavity loss and interferometer contrast using Zernike transforms and Laguerre-Gauss transforms as input

overlapzlg.f

Overlap integrals of Zernike functions with Laguerre-Gauss functions

zerncorr.f

Cross correlation of phase maps in terms of Zernike functions, comparison of phase maps

2dmap.f

Phase map analysis: rms, peak-peak, midpoint averages, 1d and 2d fourier transforms, Zernike transforms, Laguerre-Gauss transforms, phase map cleaning by removal of Zernike functions removal of Laguerre-Gauss functions

zygoconvg.f

Manipulation of Zygo phase maps from different instruments into standard form for analysis stray light maps and path history files.

edgediffloss.f

Diffraction loss and mode mixing by finite aperture mirrors.

fakemir.f

Method of generating different fake wavefront surfaces that have the same spatial power spectrum but different surfaces

SYSTEM MODELS

gravnoiseplot.f, gnp2.f gravnoiserms.f

Overall detector noise power budget including: shot noise for a variety of interferometer configurations, thermal noise from substrates, support wires, final stages of isolation system, coupling from vertical to horizontal, seismic noise from measured isolation systems,

modeled idealized systems with arbitary number of stages, magnetic controller noise, vacuum residual gas fluctuations, radiation pressure noise, frequency and amplitude noise in unbalanced interferometers naturally occurring gravity gradient noise, electronics noise in photodetector. gnp2 and gravnoiseplot give results in h(f) while gravnoiserms in h(rms).

Surface Power Spectra

The power spectra are parametrized by the prescription given in Church, Takacs and Leonard (SPIE Vol 1165 (1989)) for isotropic fractal surfaces. The one dimensional power spectrum, determined from data taken along a profilometer scan or a line in an interferometric phase map, is represented by

$$S_1(f_x) = \frac{A}{(1 + (2\pi f_x l_{cor})^2)^{c/2}}$$

The one dimensional power spectrum, S_1, and the coefficient A are expressed in units of (waves (5145A))^2 cm. l_{cor} is the surface correlation length in cm. $f(x)$ is the spatial frequency on the surface in cm^{-1} also referred to as wavenumbers. The representation of real surfaces will require different spectral models for the large, mid and small spatial scales.

The isotropic two dimensional power spectrum associated with S_1 is given by

$$S_2(f) = \frac{\Gamma((c+1)/2)}{\Gamma(c/2)} \frac{\sqrt{\pi} l_{cor} A}{(1 + (2\pi f l_{cor})^2)^{(c+1)/2}}$$

f is the isotropic spatial frequency $f = \sqrt{f_x^2 + f_y^2}$. $S_2(f)$ is expressed in units of (waves (5145A))^2 cm^2

The mirror BRDF depends on the two dimensional power spectrum and optical wavelength

$$BRDF = \frac{dP_{scat}}{d\Omega * P_{inc}} = \frac{16\pi^2}{\lambda^2} S_2(f)$$

The grating relations couple the scattering angle and surface spatial frequency. At angles where $\theta \approx \sin(\theta)$, the spatial frequency, optical wavelength and the scattering angle are related as

$$\theta \approx \lambda f$$

so that the BRDF can be expresed in terms of the scattering angle (incident beam assumed at normal incidence to the surface) by

$$BRDF = \frac{dP_{scat}(\theta)}{d\Omega * P_{inc}} = \frac{16\pi^{5/2}}{\lambda^2} \frac{\Gamma((c+1)/2)}{\Gamma(c/2)} \frac{l_{cor} A}{(1 + (2\pi\theta l_{cor}/\lambda)^2)^{(c+1)/2}}$$

The one and two dimensional power spectra are designed to give the same surface variance in waves^2

$$\frac{\sigma^2}{\lambda^2} = \int_0^\infty S_1(f_x) df_x = 2\pi \int_0^\infty S_2(f) f\, df = \frac{A}{2\sqrt{\pi}(c-1) l_{cor}} \frac{\Gamma((c+1)/2)}{\Gamma(c/2)}$$

ANALYTIC PERTURBATION METHOD

Purpose

From measured optical phase maps of individual components:

- Calculate contrast defect, $1 - C$, at antisymmetric port
- Calculate cavity loss, α
- Calculate optical fields in entire interferometer (planned)

Method

1. To interact with optics industry, convert phase maps to expansion in Zernike functions - scaling factor is aperture radius, R.

$$\psi(r,\theta) \;=\; a_{nl}\; Z_{nl}(r,\theta)$$

2. Choose cavity parameters: $g_1,\ g_2, T_{\rm m}$ and cavity Laguerre Gauss eigenfunctions $L_{pm}(r,\theta)$ - scaling factor is ω.

3. Excitation field is assumed to be L_{00}

4. Project L_{00} field excited phase map into Laguerre Gauss functions

$$\psi_{pm} \;=\; a_{nl} \;<\; pm \mid nl \mid 00 \;>\; L_{pm}$$

5. Perturbation excitation function; for example, transmission amplitude components

$$t_{pm} \;=\; t\,(1 \;+\; i\psi_{pm})$$

6. Multiply by cavity transfer function using appropriate Guoy phase for each cavity eigenfunction

Reflected field

Internal field

7. First order estimates of contrast defect and loss:

$$1 - C \;\approx 2 \sum_{p,m} I_{pm}(\text{refl})/I_{00} \qquad \alpha \;=\; \sum_{p,m} I_{pm}(\text{internal})/I_{00}$$

Method applies to both phase and amplitude perturbations, phase perturbations more important

The total scattering loss by the surface is related to the surface variance

$$\frac{P_{\text{total scat}}}{P_{\text{inc}}} = 16\pi^2 \frac{\sigma^2}{\lambda^2}$$

NOTE: The one dimensional power spectra in some commercial software is given in units of microns^3 and the spatial frequencies are given in microns^{-1}. The two dimensional power spectra are given in units of microns^4. The conversion of the power spectra used in these specifications to those using microns as the basis are the following:

$$S_1(\mu\text{m}^{-1}) = 2.65 \times 10^3 \; S_1(\text{cm}^{-1})$$

$$S_2(\mu\text{m}^{-1}) = 2.65 \times 10^7 \; S_2(\text{cm}^{-1})$$

SURFACE SPECIFICATION FOR THE LIGO ARM CAVITY MIRRORS

R. Weiss November 1, 1993

Introduction : The document presents the surface specifications for the initial LIGO interferometer arm cavity mirrors. The specifications are divided broadly into three spatial scales.

20 - 0.3 cm : The spatial scale (*large*) that primarily determines the cavity field distribution and thereby the interferometer contrast and one component of the diffractive cavity losses. Perturbations on scales 2 cm and shorter have diffracted components that fall outside the mirror radius in the arm cavities.

0.3 - 0.008 cm : The spatial scale (*mid*) that primarily contributes to the scattered light in the LIGO beam tubes producing phase noise through modulation by interaction with the walls and baffles. The mirror perturbation power spectra on these spatial scales are likely to be the same for all the mirrors so that the primary effect in the arm cavities is expected to be cavity loss rather than interferometer contrast defect.

$\leq$ .008 cm: The spatial scale (*small*) which in the LIGO contributes primarily diffractive arm cavity loss and to the interferometer contrast defect if the power spectrum on these spatial scales is different for the mirrors in the two arm cavities.

Some of the specifications are inconsistent with each other since they have been arrived at from different considerations. The specification is then determined by the more rigorous condition. A specific example are the allowed higher order Zernike amplitudes, these are larger than the values specified by the surface power spectrum. The inconsistency comes about because different performance criteria have been used. In the case of the Zernike decompositions, the interferometer contrast defect is the driver, while for the power spectrum specification, it is the scattering.

NOTE: A separate issue, not considered in this specification, is the effect from mid and small scale perturbations on the small beam tests that may be performed in cavity ring down or laboratory absorption measurements.

ANALYTIC MODELING (2)

EINSTEIN SOW CONVENTION

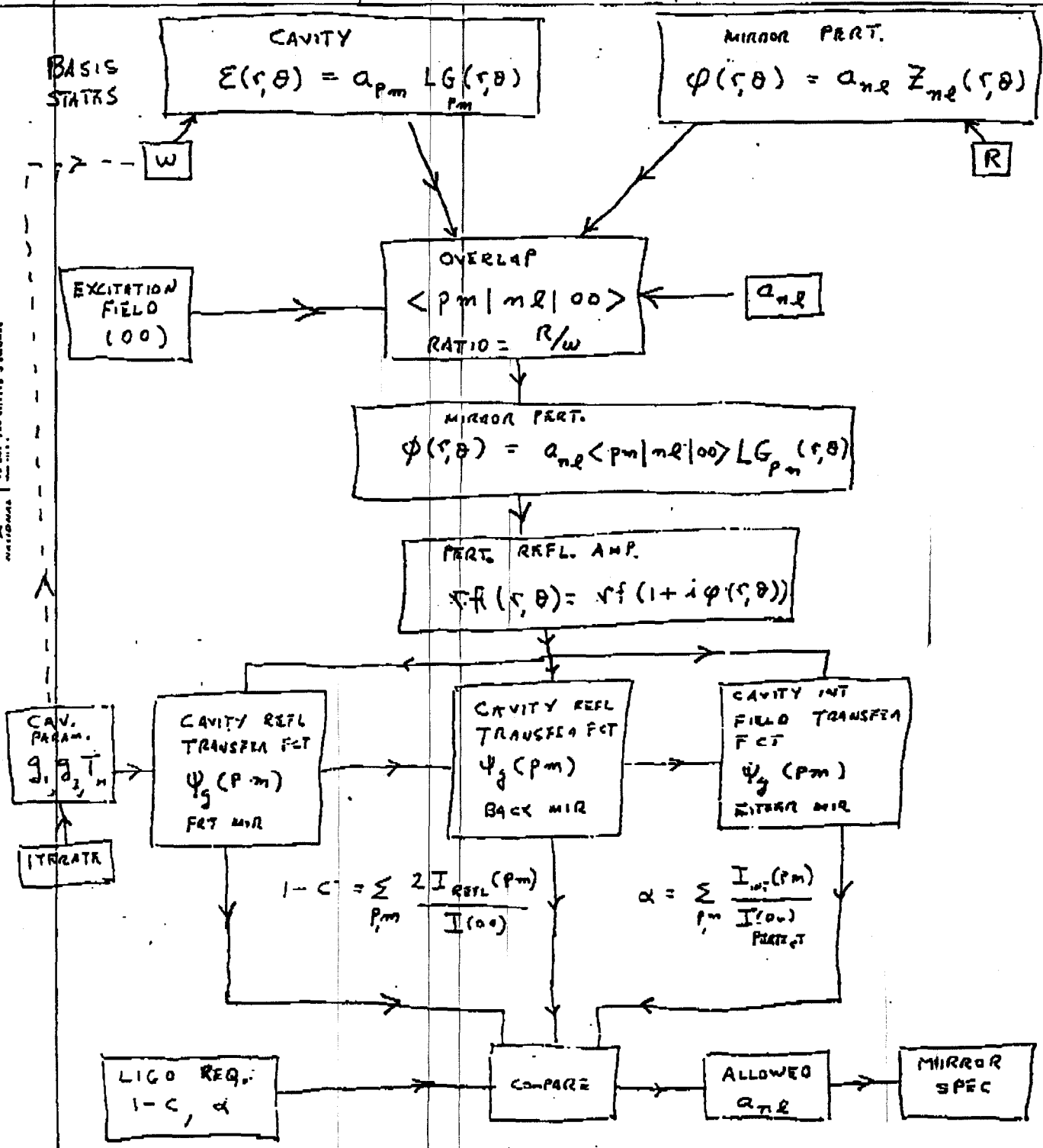

TO DO

- CONFIRM WITH NUMERICAL MODELING
- INVESTIGATE INDUSTRIAL CAPABILITIES — DISTRIBUTION OF $a_{n\ell}$

Rear arm cavity mirror - spherical

Zernike sums over a 10 cm radius aperture

$$\sum_{n=8}^{\infty} a_{n,0}^2 \leq \frac{(1-C)}{(960)} \leq 3\times 10^{-6}$$

$$\sum_{n=18}^{\infty} a_{n,2}^2 \leq \frac{(1-C)}{(478)} \leq 6\times 10^{-6}$$

$$\sum_{n=24}^{\infty} a_{n,4}^2 \leq \frac{(1-C)}{(270)} \leq 1\times 10^{-5}$$

$$\sum_{n=24}^{\infty} a_{n,6}^2 \leq \frac{(1-C)}{(120)} \leq 2\times 10^{-5}$$

Zernike sums over a 5 cm radius aperture

$$\sum_{n=4}^{\infty} a_{n,0}^2 \leq \frac{(1-C)}{(490)} \leq 6\times 10^{-6}$$

$$\sum_{n=8}^{\infty} a_{n,2}^2 \leq \frac{(1-C)}{(230)} \leq 1\times 10^{-5}$$

$$\sum_{n=10}^{\infty} a_{n,4}^2 \leq \frac{(1-C)}{(130)} \leq 2\times 10^{-5}$$

$$\sum_{n=18}^{\infty} a_{n,6}^2 \leq \frac{(1-C)}{(100)} \leq 3\times 10^{-5}$$

Weighted Laguerre - Gauss sums

$$\sum_{p=2}^{\infty}\sum_{m=0}^{p} b_{p,m,0,0}^2 \leq \frac{(1-C)}{4970} \leq 6\times 10^{-7} \quad p,\ m \text{ even}$$

Sagitta match of spherical mirrors

$$\frac{\Delta h}{\lambda} \leq 1.6\sqrt{(1-C)} \leq 0.08$$

THE SURFACE SPECIFICATIONS

Front arm cavity mirror - flat

Zernike sums over a 10 cm radius aperture

$$\sum_{n=8}^{\infty} a_{n,0}^2 \leq \frac{(1-C)}{(578)} \leq 5 \times 10^{-6}$$

$$\sum_{n=18}^{\infty} a_{n,2}^2 \leq \frac{(1-C)}{(288)} \leq 1 \times 10^{-5}$$

$$\sum_{n=24}^{\infty} a_{n,4}^2 \leq \frac{(1-C)}{(162)} \leq 2 \times 10^{-5}$$

$$\sum_{n=24}^{\infty} a_{n,6}^2 \leq \frac{(1-C)}{(72)} \leq 4 \times 10^{-5}$$

Zernike sums over a 5 cm radius aperture

$$\sum_{n=4}^{\infty} a_{n,0}^2 \leq \frac{(1-C)}{(300)} \leq 1 \times 10^{-5}$$

$$\sum_{n=8}^{\infty} a_{n,2}^2 \leq \frac{(1-C)}{(140)} \leq 2 \times 10^{-5}$$

$$\sum_{n=10}^{\infty} a_{n,4}^2 \leq \frac{(1-C)}{(80)} \leq 3 \times 10^{-5}$$

$$\sum_{n=18}^{\infty} a_{n,6}^2 \leq \frac{(1-C)}{(60)} \leq 5 \times 10^{-5}$$

Weighted Laguerre - Gauss sums

$$\sum_{p=2}^{\infty} \sum_{m=0}^{p} b_{p,m,0,0}^2 \leq \frac{(1-C)}{4970} \leq 6 \times 10^{-7} \quad p,\ m \text{ even}$$

$$\sum_{p=1}^{\infty} \sum_{m=1}^{p} b_{p,m,0,0}^2 \leq \frac{(1-C)}{1264} \leq 2 \times 10^{-6} \quad p,\ m \text{ odd}$$

Power Spectrum Parameters for Both Mirrors

Spatial frequency range: 3 - 125 cm^{-1}

Power law exponent: $c = 1$

Correlation length: $l_{cor} \geq 1 \times 10^{-1}$ cm

Power spectrum amplitude coefficient: $A \leq 2 \times 10^{-8}$ waves(5145A)^2 cm

Surface variance: $\frac{\sigma^2}{\lambda^2} = \int_3^{125} S_1(f_x) df_x \leq 1.4 \times 10^{-7}$

Surface roughness rms (in band): $\sigma \leq 2$ Angstroms

Spatial frequencies $f_x \geq 125$ cm^{-1}

Surface variance: $\frac{\sigma^2}{\lambda^2} = \int_{125}^{\infty} S_1(f_x) df_x \leq 1 \times 10^{-6}$